Check for updates

Received: 18 July 2019 | Accepted: 18 June 2020

DOI: 10.1002/stem.3256

EMBRYONIC STEM CELLS/
INDUCED PLURIPOTENT STEM CELLS

STEM CELLS

DNMT3B deficiency alters mitochondrial biogenesis and α-ketoglutarate levels in human embryonic stem cells

Artur Cieslar-Pobuda[1,2] | Theresa D. Ahrens[1] | Safak Caglayan[1] | Sidney Behringer[3] | Luciana Hannibal[3] | Judith Staerk[1,4]

[1]Centre for Molecular Medicine Norway, Nordic EMBL Partnership, University of Oslo and Oslo University Hospital, Oslo, Norway

[2]Department of Cancer Immunology, Institute for Cancer Research, Oslo University Hospital, Oslo, Norway

[3]Laboratory of Clinical Biochemistry and Metabolism, Department of General Pediatrics, Adolescent Medicine and Neonatology, Faculty of Medicine, Medical Center - University of Freiburg, Freiburg, Germany

[4]Department of Haematology, Oslo University Hospital, Oslo, Norway

Correspondence
Judith Staerk, PhD, Centre for Molecular Medicine Norway, University of Oslo, 0318 Oslo, Norway.
Email: judith.staerk@ncmm.uio.no

Funding information
Norges Forskningsråd, Grant/Award Number: 240051; European Union Seventh Framework Programme (FP7-PEOPLE-2013-COFUND), Grant/Award Number: 609020; University of Oslo, Norway; Regional Health Authority for South-Eastern Norway

Abstract

Embryonic stem cell renewal and differentiation is regulated by metabolites that serve as cofactors for epigenetic enzymes. An increase of α-ketoglutarate (α-KG), a cofactor for histone and DNA demethylases, triggers multilineage differentiation in human embryonic stem cells (hESCs). To gain further insight into how the metabolic fluxes in pluripotent stem cells can be influenced by inactivating mutations in epigenetic enzymes, we generated hESCs deficient for de novo DNA methyltransferases (DNMTs) 3A and 3B. Our data reveal a bidirectional dependence between DNMT3B and α-KG levels: a-KG is significantly upregulated in cells deficient for DNMT3B, while DNMT3B expression is downregulated in hESCs treated with α-KG. In addition, DNMT3B null hESCs exhibit a disturbed mitochondrial fission and fusion balance and a switch from glycolysis to oxidative phosphorylation. Taken together, our data reveal a novel link between DNMT3B and the metabolic flux of hESCs.

KEYWORDS
cell biology, developmental biology, embryonic stem cells, methylation

1 | INTRODUCTION

DNA methylation is an epigenetic modification in which a methyl group from S-adenosyl-L-methionine is transferred to the C5 position of cytosine in CpG dinucleotides. Epigenetic marks modulate the chromatin structure, replication timing and transcriptional control,[1-4] and regulate the activation and repression of genes involved in stem cell function and lineage specification.[5-7]

DNA methylation is catalyzed by the DNA methyltransferases (DNMTs) protein family: DNMT1 is responsible for maintenance of DNA methylation,[8] while DNMT3A and DNMT3B act as de novo methyltransferases.[9] Inactivation of any of the three DNMTs in mouse ESCs reduces global DNA methylation but has no detectable effect on the viability or proliferation of ESCs in culture. In contrast, inactivation of DNMTs in vivo causes abnormal embryonic development and a recessive lethal phenotype.[10,11] In human embryonic stem cells (hESCs), inactivation of DNMT1 results in rapid cell death,[12] while hESCs expressing catalytically inactivate DNMT3A and DNMT3B are viable.[12]

Cell fate is also influenced by the cell's metabolism. Small metabolites such as α-ketoglutarate (α-KG) serve as substrates or cofactors

This is an open access article under the terms of the Creative Commons Attribution-NonCommercial-NoDerivs License, which permits use and distribution in any medium, provided the original work is properly cited, the use is non-commercial and no modifications or adaptations are made.
© 2020 The Authors. STEM CELLS published by Wiley Periodicals LLC on behalf of AlphaMed Press.

for epigenetic modifiers such as the ten-eleven translocation (TET) enzymes and Jumonji family histone demethylases.[13] An elevated ratio of α-KG to succinate has been shown to promote histone and DNA demethylation and to maintain pluripotency in naive mouse ESCs,[14] while in primed hESCs, α-KG leads to an early multilineage differentiation.[15] The availability of α-KG and other metabolites relies on mitochondrial function mainly through the Krebs cycle,[16] and the maturation of mitochondria and a metabolic switch from glycolysis to oxidative phosphorylation have previously been associated with ESC differentiation.[17]

Here, we show that absence of DNMT3B leads to significantly elevated isocitrate dehydrogenase (IDH) and α-KG levels. Vice versa, an increase in α-KG levels leads to a downregulation of DNMT3B. Under both conditions, we find increased expression of transcription factors (TFs) that are key for early neuronal lineage differentiation. Taken together, we uncover a previously unrecognized role for DNMT3B in tuning the metabolic poise of hESCs.

Significance statement

The current study reveals a novel link between DNMT3B and the metabolic flux in human embryonic stem cells. Loss of DNMT3B disrupts the cells mitochondrial fusion and fission balance, reduces mitochondrial DNA levels, and elicits a switch from glycolysis to oxidative phosphorylation. The authors further show that loss of DNMT3B leads to an overexpression and hyperactivity of isocitrate dehydrogenases and buildup of α-ketoglutarate (α-KG), as well as a significant upregulation of transcription factors during early neural differentiation. The observed increase in α-KG levels can be reversed by re-expression of DNMT3B, demonstrating that its dysregulation is a direct consequence of DNMT3B-deficiency.

2 | MATERIALS AND METHODS

2.1 | hESC culture

The hESC lines H13 (male), H9 and WA#22 (both female) were obtained from the WiCell Research Institute (Madison, Wisconsin) and cultured on mitomycin-C treated mouse embryonic fibroblasts as described.[18] Cells were passaged using 1 mg/mL collagenase type IV (Life Technologies).

2.2 | Generation of genetically modified hESCs

Targeted deletion of *DNMT3A* and *DNMT3B* in hESCs was achieved using CRISPR-Cas9 technology. Oligonucleotides were designed using the webtool http://crispr.mit.edu/, and were cloned into px330-U6-Chimeric_BB-CBh-hSpCas9 (a gift from Feng Zhang [Addgene plasmid # 42230]) as described.[19] Primer sequences are listed in Table S1.

For the rescue experiment, the DNMT3B cDNA (pcDNA3/Myc-DNMT3B1, a gift from Arthur Riggs [Addgene plasmid # 35522][20]) was cloned into the pAAVS1-P-CAG-DEST vector, a gift from Knut Woltjen (Addgene plasmid #80490[21]), and targeted to the AAVSI locus[22] in DNMT3B−/− hESCs.

Twenty-four hours prior to electroporation, hESCs were cultured in the presence of 10 μM Rho Kinase (ROCK)-inhibitor (Y-27632; ATCC). 5×10^6 single cell hESCs resuspended in 500 μL Optimem (Life Technologies) were electroporated using 15 μg of each CRISPR plasmid (200 V, 500 μF, 0 Ω, 0.4 cm cuvettes). After, cells were plated in hESC medium with 10 μM ROCK-inhibitor for 48 hours. To generate AAVSI-DNMT3B hESCs, cells were selected in 0.5 μg/mL puromycin, and individual colonies were picked, expanded, and genotyped as described.[21] Positive clones were subjected to Southern blot to ensure single integration as described.[21]

2.3 | Genotyping

hESCs were lysed in 500 μL DNA lysis buffer (100 mM Tris pH 8.0, 5 mM EDTA, 0.2% SDS, 200 mM NaCl, 200 μg/mL proteinase K) overnight at 55°C, and precipitated using isopropanol. Genomic DNA was resuspended in 10 mM Tris pH 8.0, 0.1 mM EDTA, and incubated at 55°C overnight. Deletion of exon 4 of DNMT3A (wt: 1026 bp; targeted allele: 370 bp) and exon 2 of DNMT3B (wt: 580 bp; targeted allele: 418 bp) deficient hESC clones were verified by polymerase chain reaction (PCR) analysis and sequencing as described below. Primer sequences are listed in Table S1.

2.4 | Quantification of DNA modifications using Liquid Chromatography with tandem mass spectrometry (LC-MS/MS)

DNA modifications were quantified using LC-MS/MS as previously described.[23]

2.5 | Lineage differentiation into the three germ layers

Trilineage differentiation was performed as previously reported[12] with minor modifications. Undifferentiated hESCs were grown on matrigel (Corning) for 2 days in hESC medium before directed differentiation was induced using lineage specific medium:

Ectoderm medium: 15% Knockout Serum Replacement, 1% MEM Nonessential Amino Acids Solution, 1% antibiotic-antimycotic solution, 55 μM 2-mercaptoethanol (all Life Technologies), 2 μM A83-01, 2 μM Dorsomorphin (Sigma), 2 μM PNU-74654 (Selleckchem) in Neurobasal Medium (Life Technologies).

Endoderm medium: 100 ng/mL Activin A (Miltenyi Biotec), 2 mM LiCl (Sigma), 0.5% fetal bovine serum (FBS (Gibco)), 1% GlutaMAX Supplement, MEM Nonessential Amino Acid, 1% antibiotic-antimycotic solution, 55 μM 2-mercaptoethanol (all Life Technologies) in RPMI medium (Sigma).

Mesoderm medium: 100 ng/mL Activin A, 10 ng/mL basic fibroblast growth factor, 100 ng/mL bone morphogenetic protein 4, 100 ng/mL vascular endothelial growth factor (all Miltenyi Biotec), 0.5% FBS (Gibco), MEM Nonessential Amino Acid, 1% antibiotic-antimycotic solution, 1% GlutaMAX Supplement, 55 μM 2-mercaptoethanol (all Life Technologies) in dulbecco's modified eagle's medium (DMEM)/F12 (Sigma) for 24 hours. For the remaining 4 days, the same medium without Activin A was used.

2.6 | Cell proliferation assay

Live Cell Analysis System (IncuCyte) was used to measure the doubling times of hESCs. Shortly, hESC were dissociated into single cells and 10 000 cells were seeded per Matrigel-coated 48-well in hESC medium with 10 μM ROCK inhibitor. Doubling times were determined using the IncuCyte Live Cell Analysis System and IncuCyte Zoom software.

2.7 | Mitochondrial respiration measurements

Oxygen consumption rate (OCR) and extracellular acidification rate (ECAR) were determined using the XF Cell Mito Stress Test and XFe96 Extracellular Flux Analyzer (Seahorse, Agilent Technologies). 20 000 hESCs/well were seeded onto a Matrigel-coated XF96 cell culture microplate (Agilent) and cultured overnight in hESC medium supplemented with 10 μM ROCK inhibitor. One hour before the assay culture medium was changed to XF DMEM Medium, pH 7.4 containing 2 mM glutamine, 1 mM pyruvate, and 10 mM glucose (Seahorse, Agilent Technologies). Selective inhibitors of mitochondrial electron transport chain were injected to achieve the final concentrations of Oligomycin (1 μM), Carbonyl cyanide-4 (trifluoromethoxy) phenylhydrazone (FCCP [2 μM]), and rotenone/antimycin A (0.5 μM). Basal respiration was determined as OCR before injection of oligomycin minus OCR after injection of rotenone/antimycin A. ATP-linked respiration (here noted as ATP production) was determined as OCR before oligomycin injection minus OCR after oligomycin treatment. Maximal respiration was determined as the OCR after FCCP minus nonmitochondrial OCR (OCR after rotenone/antimycin A treatment).

Values were normalized against protein concentrations (BCA protein assay kit; Thermo Fisher Scientific). Data are presented as average values from three independent experiments with at least six technical replicates in each experiment ± SEM.

2.8 | Analysis of mitochondrial morphology and DNA content

Mitochondria were stained using CellLight Mitochondria-GFP, BacMam 2.0 (Life Technologies) according to the manufacturer's instructions. Briefly, 2 μL of BacMam 2.0 reagent per 10 000 cells was added to the medium and the cells were incubated for 48 hours before being fixed for 15 minutes in 3% paraformaldehyde (PFA). Fixed cells were counterstained with 4′,6-diamidino-2-phenylindole (DAPI) and treated with mounting medium. Images were acquired using a ×60/1.4 differential interference contrast oil immersion objective on a LSM800 airyscan confocal microscope (Zeiss). Mitochondrial changes were quantified using the Mitochondrial Network Analysis toolset for ImageJ as described.[24] At least 20 randomly taken pictures of single cells for each cell type and from three independent experiments were analyzed. Values are presented as boxplots with the lower and upper limits of the box representing the first and third quartile, respectively. The bar at the center of the box indicates the median of number of branches per mitochondrial network.

Content of mitochondrial DNA by real-time PCR was analyzed using 10 ng genomic DNA. The mitochondrial genes NADH-ubiquinone oxidoreductase chain 1 (*MT-ND1*) and *MT-ND4* were quantified and normalized to nuclear gene beta-2-microglobulin (*B2M*) to determine mitochondrial to nuclear DNA copy number ratio. Experiments were performed in triplicate.

2.9 | RNA isolation and quantitative reverse transcriptase PCR analysis

Total RNA was isolated from cells using QIAzol (Qiagen) followed by chloroform (Sigma) and isopropanol precipitation. RNA was converted to cDNA using the High Capacity cDNA Reverse Transcription Kit (Applied Biosystems) and cDNA was added to reaction mix containing Power SYBR Green PCR Master Mix (Applied Biosystems) and primers. Triplicate reactions were performed for each gene in 96-well plates using a following amplification program: 2 minutes at 50°C, 10 minutes at 95°C, followed by 40 cycles of 95°C for 15 seconds and 60°C for 60 seconds using a CFX96 real-time PCR machine (BioRad). Melting curve analysis was applied to assess primer specificity for each PCR product. No nonspecific amplification or primer-dimers were detected in any of the reactions. Relative quantification of gene expression was determined using the $2^{-\Delta\Delta CT}$ approach, and normalizing input amounts to an internal control gene (*GAPDH*) and a calibrator (parental hESCs). Primer sequences are listed in Table S1.

2.10 | Immunofluorescence

Cells grown on coverslips were fixed in 3% PFA for 15 minutes and permeabilized with 0.2% Triton X-100 for 20 minutes. After 1 hour blocking with phosphate buffered saline-1% bovine serum albumin (wt/vol), cells were incubated with primary antibodies diluted in blocking solution overnight at 4°C. Cells were washed, and stained with the respective secondary antibodies conjugated with fluorophore for 1 hour, counterstained with DAPI and treated with mounting medium. Negative controls were incubated with secondary antibodies only. Images were acquired using a fluorescent microscopy (AxioVert.A1, Zeiss) and edited using ZEN imaging software (Zeiss) and ImageJ (NIH, available at http://rsb.info.nih.gov/ij). Antibodies are listed in Table S2.

2.11 | Immunoblotting

Cells were lysed in RIPA buffer with protease inhibitors and protein concentration was measured using the BCA Protein Assay (Thermo Fisher Scientific). Fifteen micrograms protein in loading buffer was denatured for 5 minutes at 95°C, and run on a 12% Criterion TGX precast gel (Biorad) at 100 V for 1.5 hours before being transferred onto a polyvinylidene fluoride membrane (Immobilon-P, Millipore) for 1 hour at 100 V. Next, the membrane was blocked with 5% nonfat dried milk powder (Biorad) in Tris-buffered saline (TBS)/0.1% Tween 20 (TBST) and incubated with primary antibodies at 4°C overnight. The membrane was washed and incubated with horseradish peroxidase-conjugated secondary antibodies for 1 hour. Super Signal West Dura Extended Duration Substrate (Thermo Fisher Scientific) was used and membranes were visualized using the ChemiDoc XRS+ (Biorad). Immunoblotting to asses DNMT3B protein expression was performed using antibody HPA001595 (Figures 1B,D and 5A), and #72335S (Figure S1C). Antibodies are listed in Table S2.

2.12 | IDH activity assay

IDH activity was assessed using the Isocitrate Dehydrogenase Activity Assay (Sigma) according to manufacturer's instructions. 1×10^6 cells were used, and experiments were repeated four times with each sample run as technical duplicate.

2.13 | TET activity assay

Total 5mC hydroxylase TET enzyme activity was assessed using the TET Hydroxylase Activity Quantification Colorimetric Kit (Abcam) according to the manufacturer's instruction. Nuclear extracts were obtained from 1×10^6 cells using the Nuclear Extraction Kit (Abcam). Experiments were repeated two times with each sample run as technical duplicate.

2.14 | α-KG and succinate assays

Levels of intracellular α-KG and succinate were determined using the α-Ketoglutarate and Succinate Colorimetric Assay Kits (both from Sigma) according to the manufacturer's instructions. 2×10^6 cells for α-KG assay and 1×10^6 cells for succinate assay were used, and experiments were repeated three times each as technical duplicate.

2.15 | Statistical analysis

Values are presented as the mean ± SD unless stated otherwise. Data were analyzed with Prism (GraphPad). Pairwise comparisons were analyzed using two-tailed Student's *t* test. For mitochondrial networks quantification, nonparametric Mann-Whitney *U* test was used to analyze difference between two groups. In all cases, $P < .05$ was considered significant.

3 | RESULTS

3.1 | Generation of DNMT3-deficient hESC lines

hESC deficient for the de novo DNMTs DNMT3A and DNMT3B were generated using CRISPR/Cas9 technology. In case of DNMT3A, we deleted exon 4 (Figure S1A), which induces a frameshift and premature stop codon in exon 5. In case of DNMT3B, a stretch of nucleotides including the transcriptional start site was deleted in exon 2 (Figure S1A,B). DNMT3AB double knockout (DNMT3AB −/−) hESCs were derived by exposing *DNMT3A−/− hESCs* to *DNMT3B* gRNAs and Cas9. Absence of DNMT3A and DNMT3B mRNA and protein expression in targeted hESCs was verified using quantitative reverse transcriptase PCR (qRT-PCR) (Figure 1A), Western blotting (Figures 1B and S1C), and immunofluorescence (Figure 1C). mRNA expression levels of *DNMT3A* were significantly lower than those of *DNMT3B* in parental WA#22 hESCs (Figure S1D), an observation in line with a previous study.[12] DNMT3A- and B-deficient hESC lines were viable and expressed common pluripotency markers Tra1-81, OCT4, and NANOG at comparable levels as WA#22 hESCs as shown by immunofluorescence (Figure 1D) and qRT-PCR analyses (Figure 1E).

3.2 | DNMT3B deficiency reduces DNA methylation and 5-hydroxymethylation levels in hESCs

Inactivation of DNMT3A and DNMT3B is expected to result in decreased level of methylated cytosines (5mC) in DNA. Lower amount of 5mC may also lead to alterations of other, downstream DNA modifications including hydroxymethylation of cytosines (5hmC). Using mass spectroscopy analysis of 5mC and 5hmC from total genomic DNA, we found that absence of DNMT3A in hESCs had no significant effect on 5mC and 5hmC levels (Figure 1F). In contrast, DNMT3B and DNMT3AB-deficient hESCs a 29% and 26% reduction of 5mC, and a 46% and 44% reduction of 5hmC levels compared to the parental WA#22 hESC line (Figure 1F).

3.3 | Absence of DNMT3B alters growth and mitochondrial respiration of hESCs

We noticed that DNMT3B−/− grew significantly slower than parental cells. Therefore, we performed automated live-cell analysis and determined the doubling times of the individual hESC lines. We found that deficiency of DNMT3B increased the doubling time of hESCs by almost 2-fold to 30 hours in DNMT3B−/− vs 18 hours in WA#22 hESCs (Figure 2A). The same was true for DNMT3AB double null hESCs, while absence of DNMT3A had no effect (Figure 2A). Since doubling times of cells may be influenced by metabolic changes, we

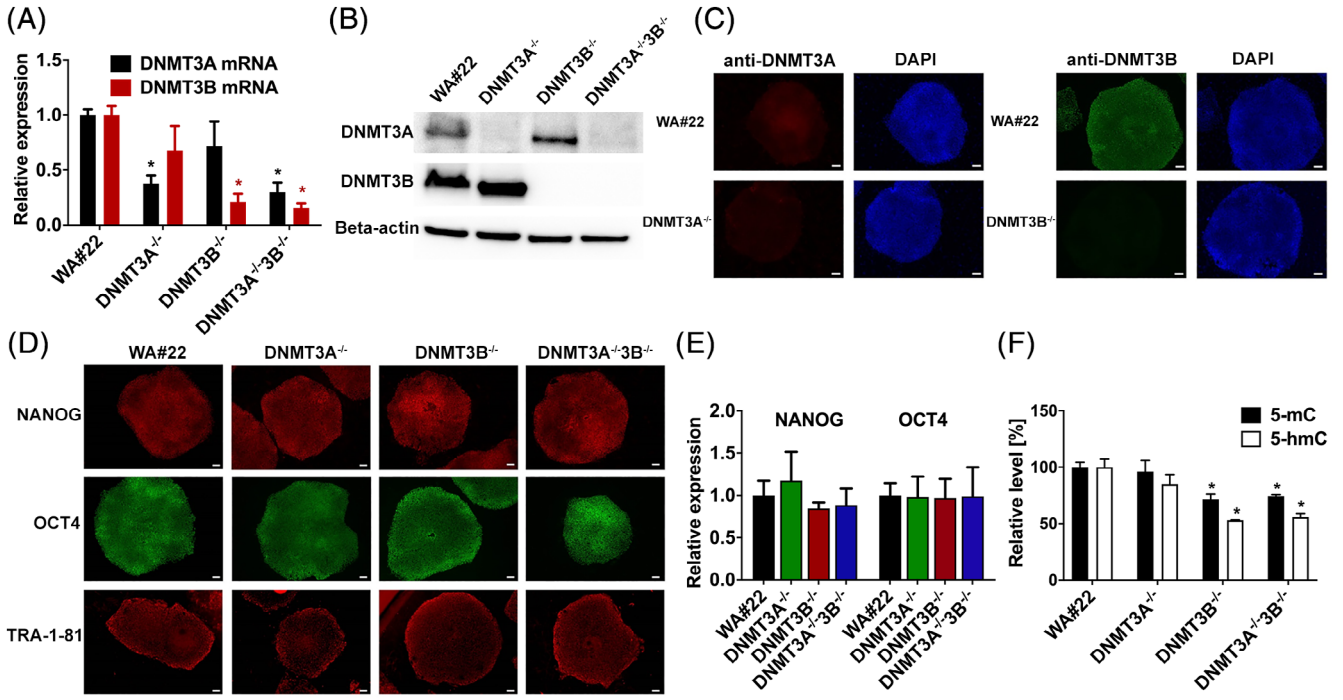

FIGURE 1 Targeted deletion of DNMT3A and DNMT3B in WA#22 hESCs. A, *DNMT3A* and *DNMT3B* mRNA expression levels in WA#22, DNMT3A−/−, DNMT3B−/−, and DNMT3AB−/− hESCs. Data are presented as means ± SD (N = 5) relative to *GAPDH* and WA#22 parental hESCs. **P* < .05. B, Immunoblot analysis of DNMT3A and DNMT3B in WA#22, DNMT3A−/−, DNMT3B−/−, and DNMT3AB−/− hESCs. Beta-actin was used as the loading control. C, Immunofluorescent staining for DNMT3A and DNMT3B in WA#22, DNMT3A−/−, DNMT3B−/−, and DNMT3AB−/− hESCs. 4′,6-diamidino-2-phenylindole (DAPI) (blue) was used to stain nuclei. Scale bars = 100 μm. D, Immunofluorescent staining for NANOG, OCT4, and TRA-1-81 in WA#22, DNMT3A−/−, DNMT3B−/−, and DNMT3AB−/− hESCs. Scale bars = 100 μm. E, *OCT4* and *NANOG* mRNA expression levels in WA#22 and genetically modified hESCs. Data are presented as means ± SD (N = 4) relative to *GAPDH* and normalized to transcript levels in WA#22 hESCs. **P* < .05. F, 5-methylcytosine (5-mC) and 5-hydroxymethylcytosine (5-hmC) levels in WA#22, DNMT3A−/−, DNMT3B−/−, and DNMT3AB−/− hESCs determined by mass spectrometry (N = 2). Data are presented as means ± SD. hESCs, human embryonic stem cells

next analyzed the mitochondrial respiration and glycolysis rates by measuring OCR (Figure 2B) and ECAR (Figure 2C), respectively. We found that DNMT3B deficiency altered the overall OCR by decreasing maximal respiration (Figure 2D), basal respiration (Figure 2E), and ATP production (Figure 2F). The reduced ECAR in DNMT3B−/− and DNMT3AB−/− hESCs points to reduced glycolysis and ATP rates and provides one possible explanation for the increased doubling time (Figure 2A).

3.4 | DNMT3B deficiency alters the mitochondrial fusion/fission balance in hESCs

Mitochondria adapt to cellular metabolism through fusion and fission.[25] Because we detected reduced oxygen consumption and glycolysis rates, we analyzed the mitochondrial morphology using mitochondrial-GFP transduced hESCs and confocal microscopy. Although there was heterogeneity, we found a significant increase of branched mitochondria in DNMT3B−/− and DNMT3AB−/− but not in WA#22 or DNMT3A−/− hESCs (Figure 2G,H).

Strikingly, the change in mitochondrial morphology in DNMT3B null hESCs was accompanied by an ~50% decrease in mRNA and protein expression of Dynamin 1 Like Protein (DNM1L/DRP1) (Figure 2I-K), an enzyme catalyzing mitochondrial fission.[26-28] The mRNA expression levels of other genes encoding proteins important for mitochondrial fusion and fission, including *OPA1*, *MTFP1*, *MFN1*, *MFN2*, *FIS1*, and *MFF* remained unchanged compared to parental WA#22 hESCs (Figure S2A).

Next, we examined mitochondrial biogenesis by measuring the copy number of mitochondrial genes NADH-ubiquinone oxidoreductase chain 1 (*MT-ND1*) and *MT-ND4*. We found significantly reduced levels of mitochondrial DNA in DNMT3B−/− and DNMT3AB−/− compared to WA#22 and DNMT3A−/− hESCs (Figure 2L). Taken together, these results show that DNMT3B is important for balanced mitochondrial biogenesis.

3.5 | Absence of DNMT3B increases α-KG levels in hESCs

Because mitochondrial biogenesis was affected in DNMT3B−/− and DNMT3AB−/− hESCs, we next analyzed components of the mitochondrial metabolism by measuring the concentration of small metabolites with known or proposed roles in hESCs

differentiation. First, we assessed the concentration of α-KG, a tricarboxylic acid cycle intermediate (Figure 3A) that plays a pivotal role as cofactor for several epigenetic enzymes. Marked elevation of α-KG was seen in DNMT3B−/− and DNMT3AB−/− but not in WA#22 and DNMT3A−/− hESCs (Figure 3B), while succinate concentration was similar in hESCs of all genotypes (Figure 3C). These data confirmed an increased ratio of α-KG to succinate in cells deficient for DNMT3B.

Since α-KG is needed for the activity of DNA and histone demethylases,[13] and we observed a significant decrease in 5hmC levels in DNMT3B−/− and DNMT3AB−/− hESCs (Figure 1F) we investigated whether this could be a consequence of increased

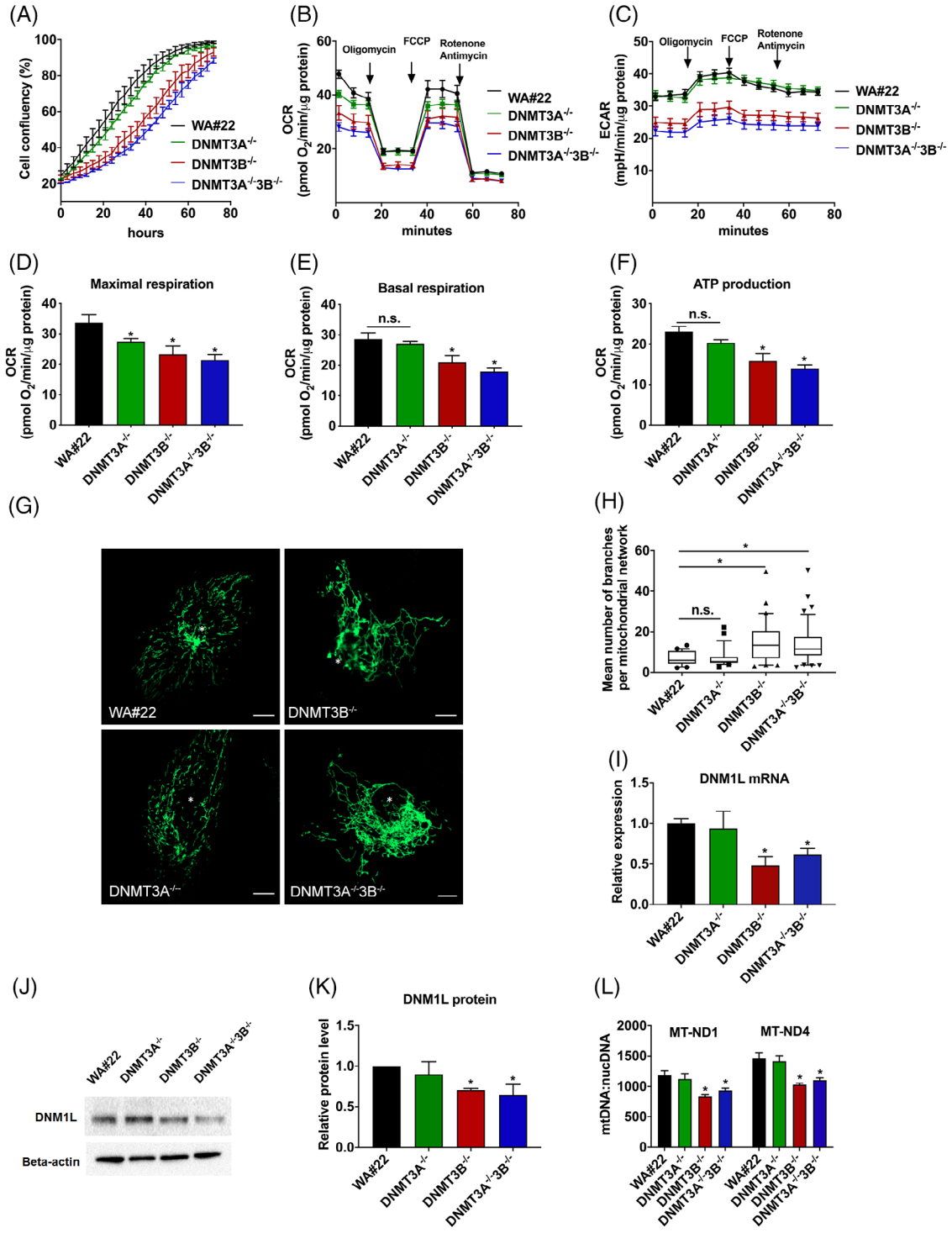

FIGURE 2 Legend on next page.

expression or activity of TET enzymes. We did neither find a significant change in *TET1* and *TET3* mRNA expression (Figure 3D), nor a significant increase in activity in DNMT3B null WA#22 hESCs although there was a trend to more activity in DNMT3B KO cells (Figure 3E). The observed reduced 5hmC levels may therefore be a combination of slightly increased TET activity and overall reduced 5mC levels.

Next, we wanted to determine the potential source of elevated α-KG to succinate ratio in DNMT3B−/− cells. Therefore, we analyzed the expression of enzymes involved in these pathways. α-KG is produced by IDHs and mitochondrial glutamate dehydrogenases (GLUDs). Moreover, the steady-state concentration of α-KG also depends on its rate of conversion to succinyl-CoA and succinate by the α-KG dehydrogenase complex (DLD, DLST, OGDH), and succinyl-CoA ligases (GDP-forming: SUCLG1, SUCLG2; ADP-forming: SUCLA2), respectively (Figure 3A). qRT-PCR analysis showed that mRNA expression levels of *IDH* enzymes were upregulated in cells deficient for DNMT3B (Figure 3F), while mRNA expression of *GLUD1*, *GLUD2*, *DLD*, *DLST*, *OGDH*, *SUCLG1*, *SUCLG2*, and *SUCLA2* was not influenced by the presence or absence of DNMT3A and DNMT3B (Figure S2B). Specifically, we observed an approximately 2-fold increase of *IDH1* and *IDH2* mRNA expression levels in DNMT3A−/− and DNMT3B−/− hESCs (Figure 3F). For *IDH3a*, *IDH3b*, and *IDH3g*, a 10- to 25-fold increase in mRNA expression levels was found in DNMT3B−/− compared to DNMT3A−/− and parental WA#22 hESCs (Figure 3F). A similar result was obtained when analyzing two additional WA#22 DNMT3B−/− clones (Figure S2C). Western blot analysis confirmed the increased IDH1, IDH3a, IDH3b, and IDH3g expression also at the protein level, while IDH2 protein levels were not increased (Figure 3G). To assess whether the observed increase in IDH protein levels had an impact on NAD^+-dependent IDH3s and $NADP^+$-dependent IDH1 and IDH2 enzymatic activities, we performed an IDH activity assay. In line with increased IDH protein expression levels, we observed an increased enzymatic activity only in DNMT3B−/− hESCs (Figure 3H,I). In addition, we showed that the activity of $NADP^+$-dependent IDHs was one order of magnitude higher than activity of NAD^+-dependent IDHs. The assay used to determine IDH activities does not distinguish between cytosolic IDH1 and mitochondrial IDH2. However, we only found increased IDH1 but not IDH2 protein levels suggesting that IDH1, next to IDH3, contributed to the increased production of α-KG.

Using trilineage differentiation to determine IDH levels in lineage cells, we found that all differentiated cells expressed comparable mRNA levels of *IDH1*, *IDH2*, and *IDH3* (Figure S2D). Thus, while IDH3 isoforms are highly expressed in DNMT3B−/− hESCs, they become downregulated during differentiation suggesting that IDH3 may play a regulatory role in hESC.

3.6 | Rescue of DNMT3B reverses the metabolic changes observed in DNMT3B null hESCs

To elucidate whether the observed gene expression and metabolic changes were directly linked to DNMT3B, we inserted the DNMT3B cDNA in the *AAVSI* locus[22] in DNMT3B−/− hESCs. We were able to partially restore *DNMT3B* mRNA (Figure 4A) and protein (Figure 4B) expression, and first analyzed the doubling time using automated live-cell analysis. Our data revealed that the doubling time in rescue cells was 23.5 hours compared to 19 hours in WA#22 parental and 30 hours in DNMT3B null hESCs (Figure 4C). Next, we measured α-KG and succinate levels and could show that in DNMT3B rescue hESCs, α-KG levels were restored to levels found in WA#22 hESCs (Figure 4D), while succinate remained unchanged (Figure 4E). The observed decrease in α-KG correlated with IDH1 and IDH3a-g mRNA expression levels similar to the ones in WA#22 hESCs (Figure 4F). When we analyzed IDH protein expression levels in DNMT3B rescue cells compared with WA#22 and DNMT3B−/− hESCs, we found similar IDH1 and IDH2 protein levels in all cells analyzed (Figure 4B).

FIGURE 2 Energy metabolism and mitochondrial morphology is altered in DNMT3B-deficient hESCs. A, Proliferation rates of hESCs quantified using an Incucyte instrument. Data are presented as means ± SEM. N = 2 independent experiments with ≥5 technical replicates for each experiment and each genotype. B, OCR (indicative of mitochondrial respiration) in WA#22, DNMT3A−/−, DNMT3B−/−, and DNMT3AB −/− hESCs. Oligomycin (1 μM, inhibits ATP synthase), FCCP (2 μM, collapses the proton gradient and disrupts the mitochondrial membrane potential), and rotenone/antimycin A (0.5 μM, complex I and III inhibitors) were sequentially applied to induce mitochondrial stress. C, ECAR (indicative of glycolysis) under mitochondrial stress in WA#22, DNMT3A−/−, DNMT3B−/−, and DNMT3AB−/− hESCs. D, Maximum respiration rates, E, basal respiration rates, and, F, ATP production in WA#22 hESCs positive or negative for DNMT3A and/or DNMT3B. Data present average values from three independent experiments with at least six technical replicates in each experiment ± SEM. *P < .05. G, Confocal microscopy images of mito-GFP transduced WA#22, DNMT3A−/−, DNMT3B−/−, and DNMT3AB−/− hESCs. * denotes nucleus. Scale bars = 10 μm. H, Quantification of branches in mitochondrial networks. Data are presented as boxplots. The lower and upper limits of the box represent the first and third quartile, respectively, and the bar at the center of the box indicates the median. Error bars show the 10% to 90% confidence interval. N = 3 experiments with at least 20 cells analyzed in each experiment. Nonparametric Mann-Whitney *U* test was used to analyze difference between two groups. *P < .05. I, *DNM1L* mRNA expression levels in WA#22 hESCs positive or negative for DNMT3A and/or DNMT3B. Data are presented as means ± SD (N = 3) relative to *GAPDH* and normalized to transcript levels in WA#22 hESCs. *P < .05. J, Immunoblot analysis of DNM1L in WA#22 hESCs positive or negative for DNMT3A and/or DNMT3B. Beta-actin was used as the loading control. K, Quantification of DNM1L protein levels in WA#22, DNMT3A−/−, DNMT3B−/−, and DNMT3AB−/− hESCs. Data are presented as means ± SD (N = 2). *P < .05. L, Quantification of mitochondrial DNA relative to nuclear DNA measured by quantitative polymerase chain reaction (q-PCR) in WA#22 hESCs positive or negative for DNMT3A and/or DNMT3B. Data are presented as means ± SD (N = 3) relative to *B2M*. *P < .05. ECAR, extracellular acidification rate; hESCs, human embryonic stem cells; n.s., not significant; OCR, oxygen consumption rate

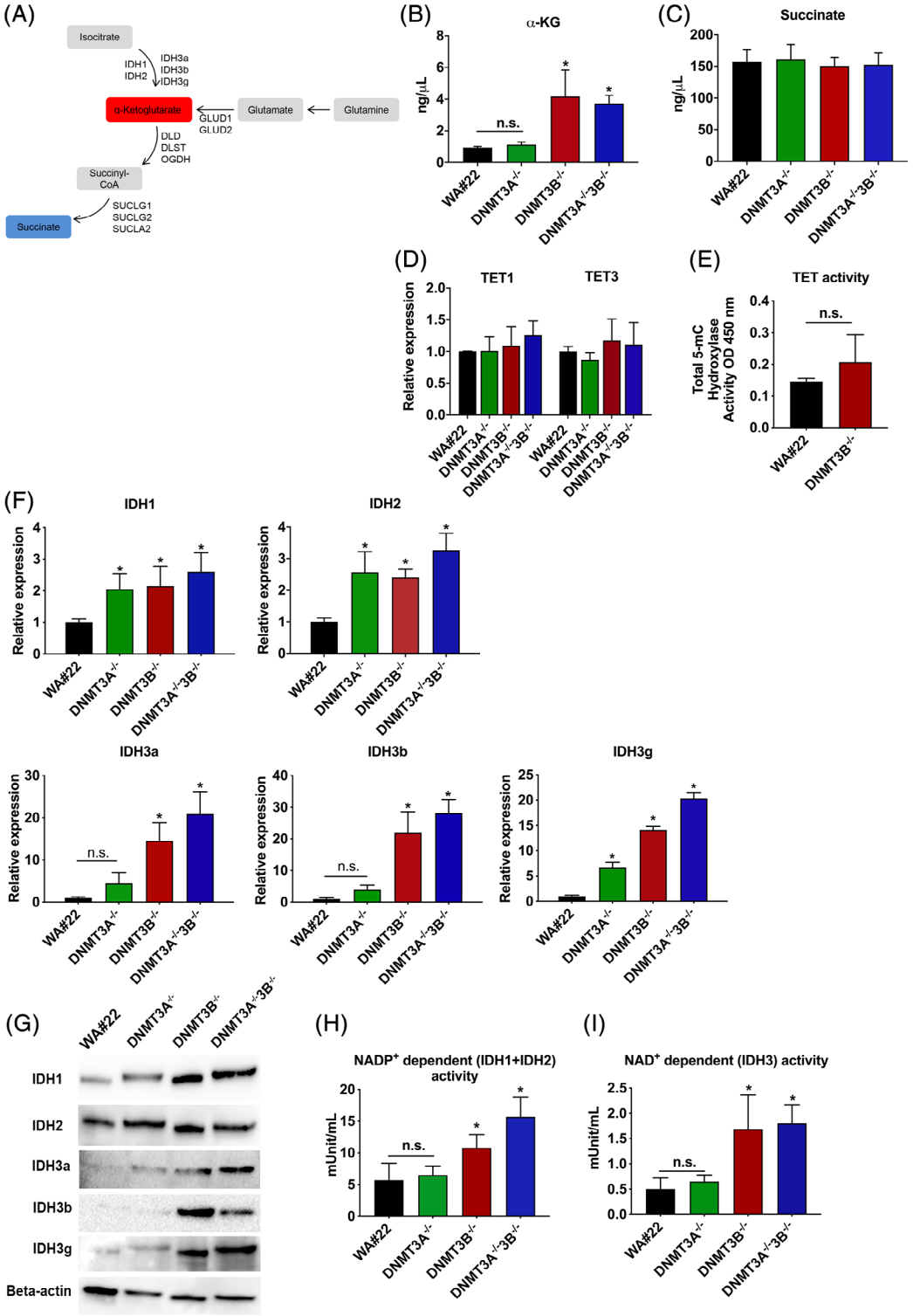

FIGURE 3 Increased α-KG production in DNMT3B-deficient hESCs. A, Schematic overview of TCA cycle and α-KG metabolism. B, Intracellular concentration of α-KG in WA#22 hESCs positive or negative for DNMT3A and/or DNMT3B. C, Intracellular concentration of succinate in hESCs. D, *TET1* and *TET3* mRNA expression levels in WA#22, DNMT3A−/−, DNMT3B−/−, and DNMT3AB−/− hESCs relative to *GAPDH* and normalized to transcript levels in WA#22 hESCs. E, Total 5-mC hydroxylase activity of TET proteins in WA#22 and DNMT3B−/− hESCs. F, *IDH1*, *IDH2*, *IDH3a*, *IDH3b*, and *IDH3g* mRNA expression levels in WA#22, DNMT3A−/−, DNMT3B−/−, and DNMT3AB−/− hESCs relative to *GAPDH* and normalized to transcript levels in WA#22 hESCs. G, Immunoblotting of IDH1, IDH2, IDH3a, IDH3b, and IDH3g in WA#22 hESCs positive or negative for DNMT3A and/or DNMT3B. Beta-actin was used as loading control. H, Activity of $NADP^+$-dependent isocitrate dehydrogenases IDH1 and IDH2. I, Activity of NAD^+-dependent isocitrate dehydrogenases IDH3s. Data in all graphs are presented as means ± SD (N ≥ 3). *P < .05. α-KG, α-ketoglutarate; hESCs, human embryonic stem cells; n.s., not significant; TCA, tricarboxylic acid; TET, ten-eleven translocation

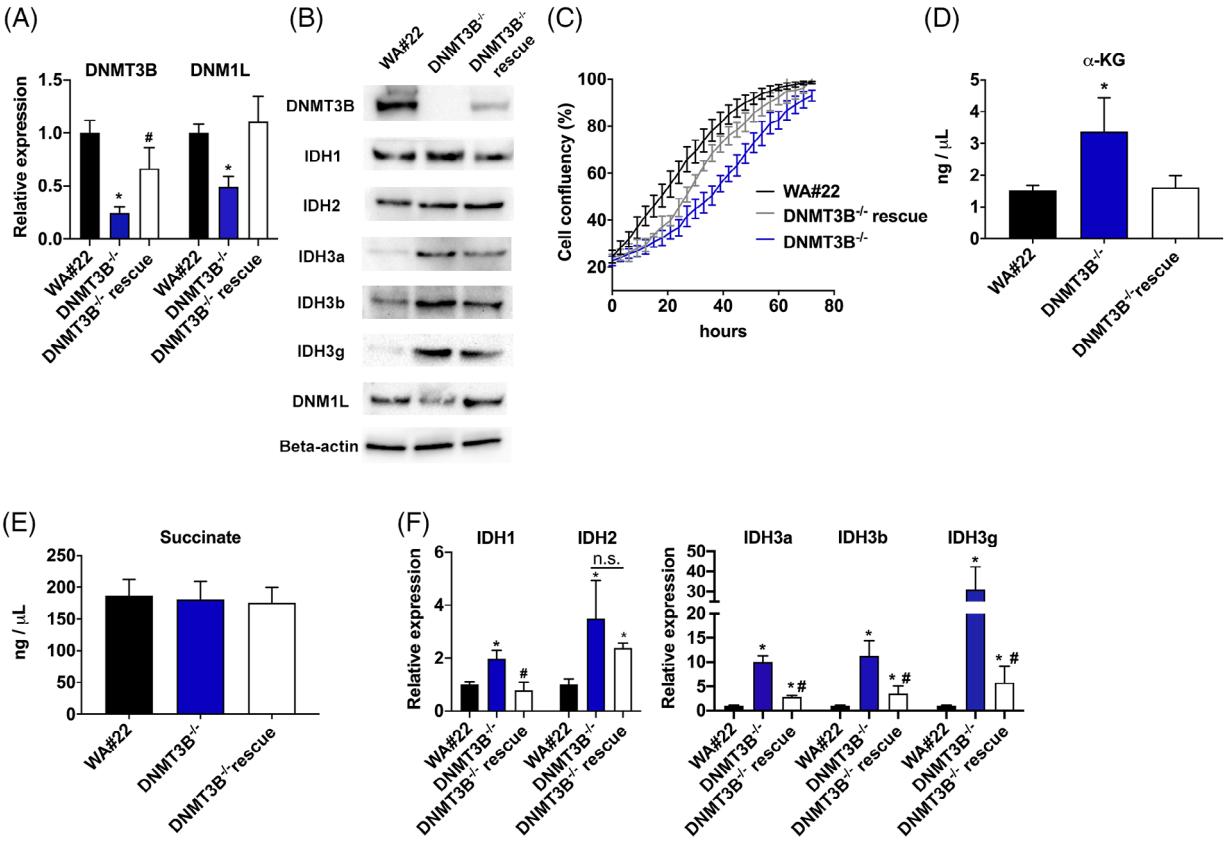

FIGURE 4 Rescue of *DNMT3B* expression restores metabolic and genetic changes. A, *DNMT3B* and *DNM1L* mRNA levels in WA#22, DNMT3B−/−, and DNMT3B-rescue hESCs relative to *GAPDH* and parental WA#22 hESCs. B, Immunoblot analysis of IDH1, IDH2, IDH3b, IDH3g, and DNM1L in WA#22, DNMT3B−/− and DNMT3B-rescue hESCs. Beta-actin was used as loading control. C, Doubling times of WA#22, DNMT3B−/− and DNMT3B-rescue hESCs quantified using an Incucyte instrument. Data are presented as means ± SEM. N = 2 independent experiments with ≥5 technical replicates for each experiment and each genotype. D, Intracellular concentration of α-KG in WA#22, DNMT3B−/− and DNMT3B-rescue hESCs. E, Intracellular concentration of succinate in hESCs. F, *IDH1*, *IDH2*, *IDH3a*, *IDH3b*, and *IDH3g* mRNA expression levels in WA#22, *DNMT3B*−/−, and *DNMT3B*-rescue hESCs relative to *GAPDH* and normalized to transcript levels in WA#22 hESCs. Data from qRT-PCR analysis, α-KG, and succinate experiments are presented as means ± SD (N = 3). $^{*}P < .05$ compared to WA#22 hESCs. $^{\#}P < .05$ compared to DNMT3B−/− hESCs. α-KG, α-ketoglutarate; hESCs, human embryonic stem cells; n.s., not significant; qRT-PCR, quantitative reverse transcriptase PCR

While IDH3b remained unchanged in rescue DNMT3B cells, we found IDH3a and IDH3g protein levels reduced although not to the levels of parental hESCs (Figure 4B). These results point to IDH3a and IDH3g as the main players in elevating α-KG levels in DNMT3B−/− hESCs. Finally, we found DNM1L protein and mRNA levels comparable to those in WA#22 cells (Figure 4A,B). Taken together, our results show that partial rescue of DNMT3B reverses the observed genetic and metabolic changes found in DBMT3B null cells, indicating that these changes are indeed a direct consequence of DNMTB deficiency.

3.7 | Metabolic changes caused by DNMT3B deficiency are conserved in other hESC lines

To exclude that the observed genetic and metabolic changes were not due to known variability between hESC lines at the epigenetic level, we generated DNMT3B null H9 and H13 hESC lines (Figures 5A and S1C) to verify our key findings. H9 and H13 DNMT3B null cells express similar *OCT4* and *NANOG* mRNA levels than the parental lines (Figure S2E). We then analyzed the doubling time using automated live-cell analysis, and demonstrated that the absence of DNMT3B in H9 and H13 hESCs increased the doubling time to 30 hours compared to 23 hours in H9 and to 31 hours compared to 25 hours in H13 hESCs (Figure 5B), respectively. Next, we analyzed mitochondrial respiration and glycolysis rates by measuring OCR. Similar to what we observed in WA#22 hESCs, DNMT3B deficiency significantly decreased OCR (Figure 5C), basal respiration (Figure 5D), maximal respiration (Figure 5E), and ATP production (Figure 5F). Moreover, mitochondrial-GFP transduced hESCs again visualized increased branching of mitochondria in DNMT3B−/− but not in the corresponding parental lines (Figure 5G). In line with this, the copy number of mitochondrial genes *MT-ND1* and *MT-ND4* were significantly reduced in DNMT3B−/− H9 and H13 hESCs (Figure 5H). We also confirmed a marked elevation of α-KG in DNMT3B−/− H9 and H13 compared to

control H9 and H13 hESCs (Figure 5I), while succinate levels did not differ between genotypes (Figure 5J). This increase in α-KG correlated with increased mRNA expression of *IDH1*, *IDH2*, as well as *IDH3a*, *IDH3b*, and *IDH3g* (Figure 5K). Similar to DNMT3B null WA#22 hESCs, we observed a disturbed mitochondrial fusion/fission balance of mitochondria in H9 and H13 DNMT3B null hESCs (Figures 2I-K). However, in DNMT3B−/− H9 and H13 hESCs, this correlated with significantly increased *OPA1* mRNA expression levels (Figure 5L) and not with downregulation of DNM1L. The mRNA expression levels of *DNM1L*, *MTFP1*, *MFN1*, *MFN2*, *FIS1*, and *MFF* were comparable in all

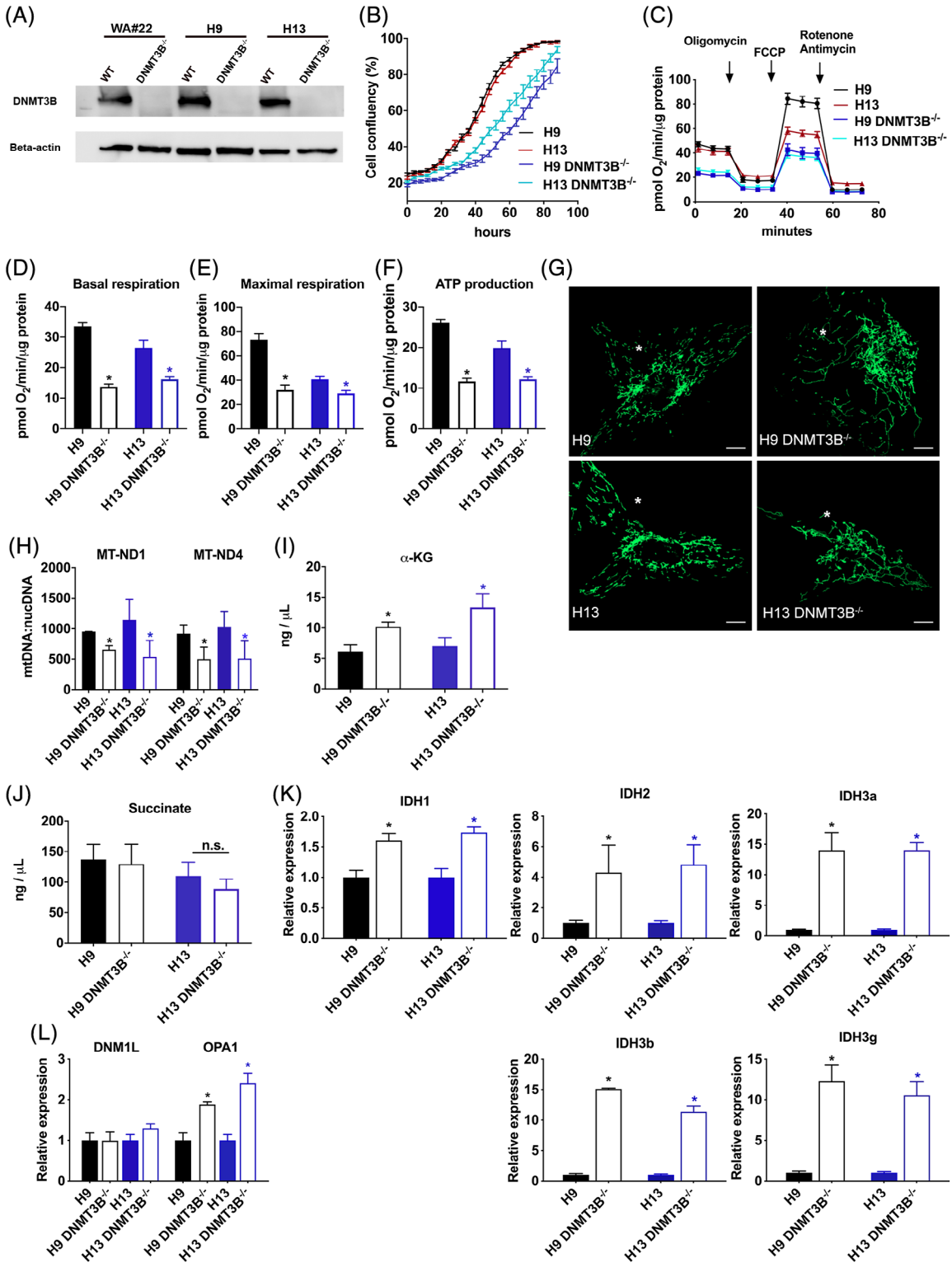

FIGURE 5 Legend on next page.

lines analyzed (Figures S3A). Taken together, our data show that the overall alterations in mitochondrial biogenesis and metabolism are indeed influenced by DNMT3B and are not caused by the (epi)genetic background of individual hESC lines.

3.8 | Transcription factors important for neural differentiation are upregulated in DNMT3B-deficient hESCs and ectoderm

Next, we assessed the differentiation potential of DNMT3−/− hESCs and generated ectodermal, endodermal, and mesodermal cells to analyze mRNA expression levels of lineage specific TFs. WT, DNMT3A −/−, and DNMT3B−/− hESCs gave rise to all three germ layers as indicated by *DLK1*, *RAX* (ectoderm), *GATA6*, *SOX17* (endoderm), and *HAND1*, *MSX1* (mesoderm) mRNA expression levels (Figure S3B). While we did not find a significant impediment toward mesoderm and ectoderm, we found significantly lower expression of GATA6 and SOX17 in both DNMT3A and DNMT3B knockout cells suggesting that DNMT3A−/− and DNMT3B−/− hESCs were less prone to differentiate into endoderm. In addition, we observed a significant upregulation of the neural TF RAX in DNMT3B−/− hESCs indicating that DNMT3B−/− hESCs have a higher propensity to form ectoderm. We then analyzed additional TFs known to be important for neuronal lineage specification. Interestingly, *PAX6*, *RAX*, and *HES5* mRNA expression levels were significantly elevated in DNMT3B-deficient hESC and early ectoderm compared to control WA#22 hESCs. For *DLK1*, *OTX2*, and *NCAM*, we noticed increased gene expression in DNMT3B−/− hESCs but not in ectoderm cells (Figure 6A). Deletion of DNMT3A did not affect the expression levels of the genes mentioned above, while DNMT3AB−/− double null cells showed a similar behavior than DNMT3B−/− cells (Figure S4). We obtained similar results during ectodermal differentiation of H9 and H13 DNMT3B −/− cells, although there were some line specific differences. For instance, *PAX*, *RAX*, *NCAM* mRNA expression was significantly increased in both H9 and H13 DNMT3B KO ectoderm (Figure 6B), while *DLK1* and *OTX2* was only significantly upregulated in H13 and *NESTIN*, *HES1*, and *HES5* in H9 DNMT3B null ectoderm (Figure 6B).

Early lineage differentiation has been reported in hESCs with elevated α-KG levels.[15] Since α-KG is upregulated in DNMT3B KO cells, we investigated whether treatment of hESCs with cell-permeable dimethyl-α-KG (dm-α-KG) leads to an upregulation of the TFs affected by deletion of DNMT3B. As shown in Figure 7A, treatment of hESCs with 6 mM or 12 mM α-KG leads to upregulation of *PAX6*, *RAX*, *DLK1*, *HES5*, and *NCAM* similar to what we observed in DNMT3B knockout cells. In contrast, *OCT4* and *NANOG* mRNA levels remained unchanged (Figure 7B). Strikingly, treatment of hESCs with α-KG led to a downregulation of DNMT3B (Figure 7B). Thus, our data reveal a link between α-KG and DNMT3B levels, a finding further supported by our rescue experiments showing that DNMT3B decreases α-KG back to levels found in parental WA#22 hESCs (Figure 4D,E).

4 | DISCUSSION

Our study shows that deletion of DNMT3B alters the metabolic flux and availability of small metabolites in pluripotent stem cells by increasing IDH activity and buildup of α-KG.

α-KG has recently been shown to accelerate early lineage differentiation of primed human pluripotent stem cells.[15,29] We also observe an upregulation of TFs involved in early ectoderm differentiation in DNMT3B null cells. Our data suggest that DNMT3B is needed to maintain balanced α-KG levels, since (a) knockout of DNMT3B increased IDH expression and α-KG levels, (b) rescue of DNMT3B restored α-KG levels back to levels found in parental hESCs, and (c) exposure of hESCs to cell-permeable dimethyl-αKG led to downregulation of DNMT3B and upregulation of lineage TFs such as PAX6, RAX, and HES5. These changes do not seem to be a consequence of a more differentiated state of the DNMT3B null hESC lines since *OCT4* and *NANOG* mRNA expression levels were comparable between different lines.

FIGURE 5 Energy metabolism, mitochondrial morphology, and α-KG production are altered in H9 and H13 hESCs positive or negative for DNMT3B. A, Immunoblotting of DNMT3B in parental and DNMT3B−/− WA#22, H9, and H13 hESCs. Beta-actin was used as the loading control. B, Doubling times of parental and DNMT3B−/− WA#22, H9, and H13 hESCs quantified using an Incucyte instrument. Data are presented as means ± SEM. N = 2 independent experiments with ≥5 technical replicates for each experiment and each genotype. C, OCR (indicative of mitochondrial respiration) in parental and DNMT3B−/− H9 and H13 hESCs. Oligomycin (1 μM), FCCP (2 μM), and rotenone/antimycin A (0.5 μM) were sequentially applied to induce mitochondrial stress. D, Basal respiration rates, E, Maximal respiration rates, and, F, ATP production in parental and DNMT3B−/− WA#22, H9, and H13 hESCs. Data present average values from three independent experiments with at least six technical replicates in each experiment ± SEM. G, Confocal microscopy images of mito-GFP transduced hESCs. Scale bars = 10 μm. H, Quantification of mitochondrial DNA relative to nuclear DNA measured by q-PCR. Data are presented as means ± SD (N = 3) relative to *B2M*. I, Intracellular concentration of α-KG in H9 and H13 hESCs positive or negative for DNMT3B. Data are presented as means ± SD (N = 3). J, Intracellular concentration of succinate in H9 and H13 hESCs positive or negative for DNMT3B. Data are presented as means ± SD (N = 3). K, *IDH1*, *IDH2*, *IDH3a*, *IDH3b*, and *IDH3g* mRNA expression levels in H9 and H13 hESCs positive or negative for DNMT3B. L, *DNM1L* and *OPA1* mRNA expression levels in parental and DNMT3B−/− WA#22, H9, and H13 hESCs. Data are presented as means ± SD (N = 3) relative to *GAPDH* and normalized to transcript levels in H9 or H13 hESCs. *$P < .05$. α-KG, α-ketoglutarate; hESCs, human embryonic stem cells; n.s., not significant; OCR, oxygen consumption rate

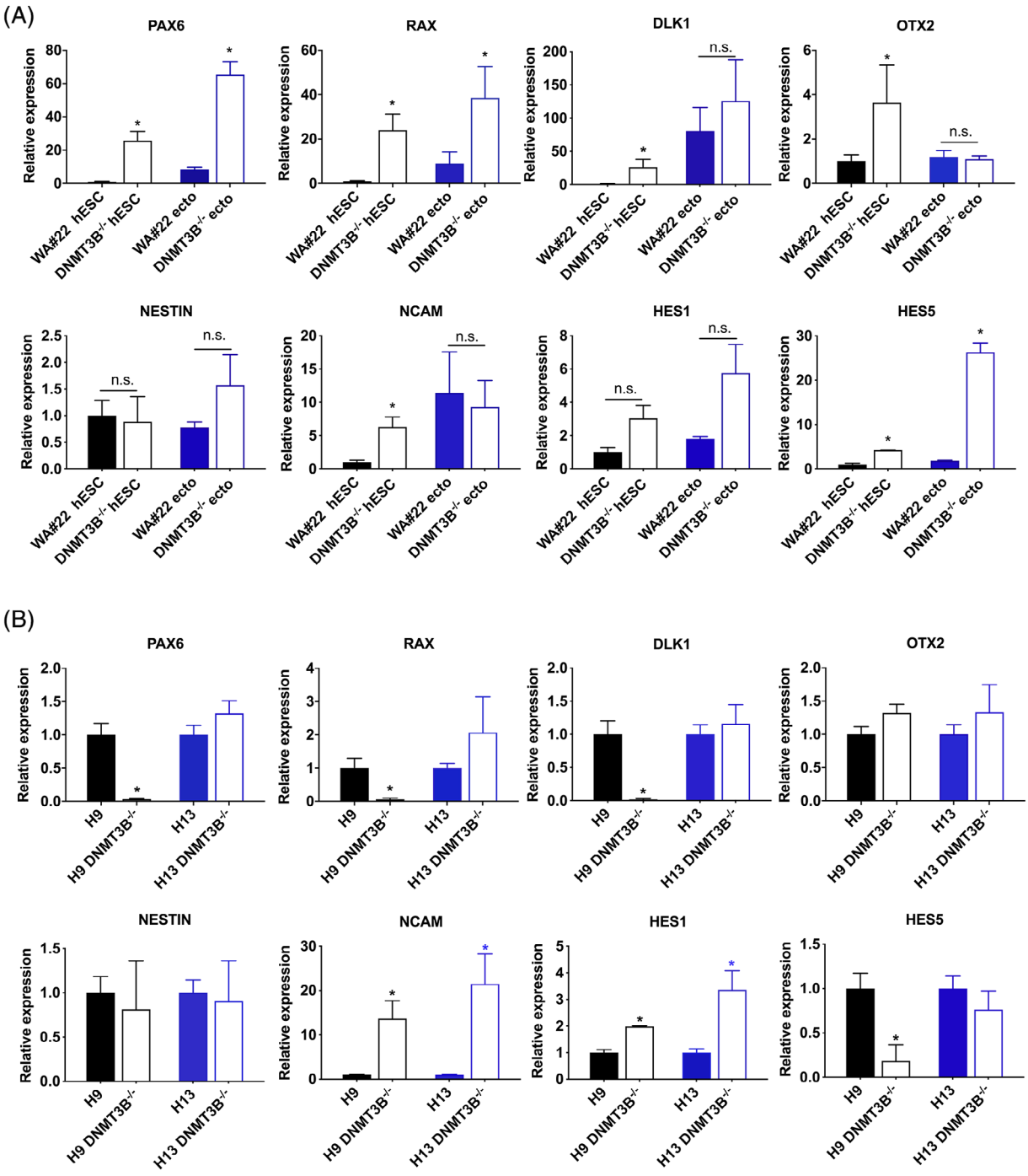

FIGURE 6 DNMT3B-deficient hESCs show higher propensity to differentiate toward ectoderm. A, *PAX6*, *RAX*, *DLK1*, *OTX2*, *NCAM*, *HES1*, *HES5*, and *NESTIN* mRNA expression levels in WA#22 and DNMT3B−/− hESCs and ectoderm. B, *PAX6*, *RAX*, *DLK1*, *OTX2*, *NCAM*, *HES1*, *HES5*, and *NESTIN* mRNA expression levels in early ectoderm derived from H9, H13, and corresponding DNMT3B null lines. Data are presented as means ± SD (N = 3) relative to *GAPDH* and normalized to transcript levels in H9 or H13 hESCs. *$P < .05$ compared to control. hESCs, human embryonic stem cells; n.s., not significant

Absence of DNMT3B correlated with an altered mitochondrial fusion/fission balance, reduced mtDNA levels, and a switch from glycolysis to oxidative phosphorylation. Stem cells rely on high glucose levels and differentiation is accompanied by a switch to oxidative phosphorylation.[30,31] Our findings suggest that DNMT3B deficiency may contribute to accelerated differentiation through a switch to oxidative phosphorylation.

Importantly, the key results obtained in this study were reproducible in three independent hESC lines demonstrating that the observed genetic and metabolic changes were not due to variability between

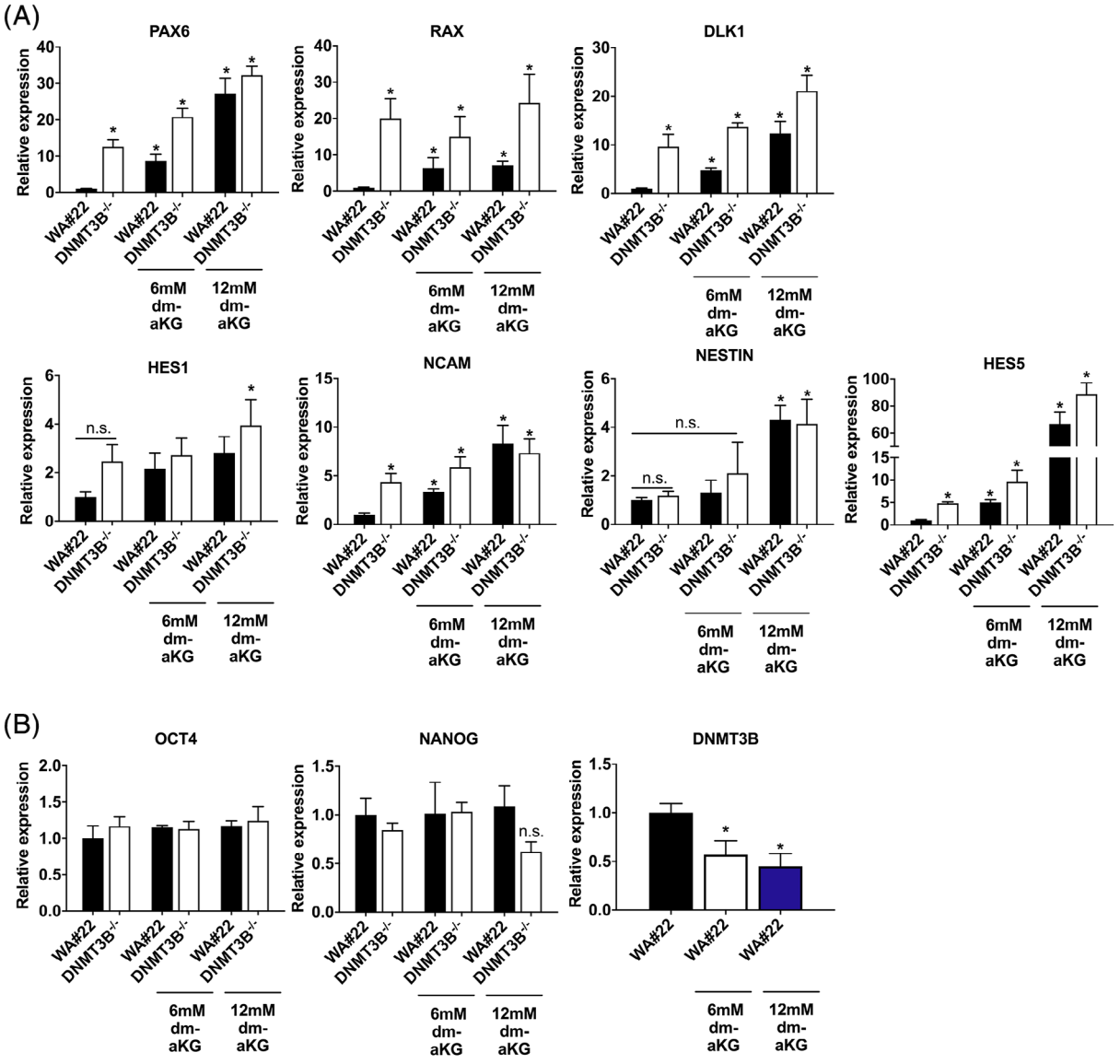

FIGURE 7 α-KG increases expression of ectodermal TFs in hESCs and reduces expression of DNMT3B. A, *PAX6*, *RAX*, *DLK1*, *OTX2*, *NCAM*, *HES1*, *HES5*, and *NESTIN* mRNA expression levels in WA#22 and DNMT3B−/− hESCs incubated for 48 hours with or without 6 mM dm-αKG, 12 mM dm-αKG. B, *OCT4*, *NANOG*, and *DNMT3B* mRNA expression levels in WA#22 and DNMT3B−/− hESCs incubated for 48 hours with or without 6 mM dm-αKG, and 12 mM dm-αKG. Data are presented as means ± SD (N = 3) relative to *GAPDH* and normalized to transcript levels in WA#22 hESCs. α-KG, α-ketoglutarate; hESCs, human embryonic stem cells; TFs, transcription factors

hESC lines on the epigenetic level. In the future, it will be important to further elucidate the crosstalk between DNMT3B, mitochondrial biogenesis, and energy metabolism and how it affects stem cell renewal and cell fate decisions.

5 | CONCLUSION

Our results demonstrate that mitochondrial biogenesis as well as the intracellular concentration and flux of α-KG that is known to affect hESC homeostasis are depending on a balanced expression of DNMT3B.

ACKNOWLEDGMENTS

Funding to J. S. is acknowledged from the Research Council of Norway, the Regional Health Authority for South-Eastern Norway, the University of Oslo, Norway, and the European Union Seventh Framework Programme (FP7-PEOPLE-2013-COFUND) under Grant 609020—Scientia Fellows. The HPLC-MS/MS analyses of DNA modifications were performed by the Proteomics and Modomics Experimental Core Facility (PROMEC), Norwegian University of Science and Technology (NTNU), Trondheim, Norway. PROMEC is funded by the Faculty of Medicine and Health Sciences at NTNU and the Central Norway Regional Health Authority, Norway.

CONFLICT OF INTEREST

The authors declared no potential conflicts of interest.

AUTHOR CONTRIBUTIONS

J.S.: generation of hESC knockout and rescue lines, study design, results interpretation, manuscript writing; A.C.-P.: generation of hESC knockout and rescue lines, study design, performed experiments, results interpretation, manuscript writing; T.D.A., S.C., S.B.: performed experiments, results interpretation; L.H.: results interpretation; All authors commented and approved the final version.

DATA AVAILABILITY STATEMENT

The data that support the findings of this study are available within the article and the online supporting information.

ORCID

Judith Staerk https://orcid.org/0000-0001-8698-6998

REFERENCES

1. Kaslow DC, Migeon BR. DNA methylation stabilizes X chromosome inactivation in eutherians but not in marsupials: evidence for multi-step maintenance of mammalian X dosage compensation. *Proc Natl Acad Sci USA*. 1987;84(17):6210-6214.
2. Li E, Beard C, Jaenisch R. Role for DNA methylation in genomic imprinting. *Nature*. 1993;366(6453):362-365.
3. Aran D, Toperoff G, Rosenberg M, Hellman A. Replication timing-related and gene body-specific methylation of active human genes. *Hum Mol Genet*. 2011;20(4):670-680.
4. Deaton AM, Bird A. CpG islands and the regulation of transcription. *Genes Dev*. 2011;25(10):1010-1022.
5. Palacios D, Summerbell D, Rigby PWJ, Boyes J. Interplay between DNA methylation and transcription factor availability: implications for developmental activation of the mouse Myogenin gene [in English]. *Mol Cell Biol*. 2010;30(15):3805-3815.
6. Polo JM, Liu S, Figueroa ME, et al. Cell type of origin influences the molecular and functional properties of mouse induced pluripotent stem cells [in English]. *Nat Biotechnol*. 2010;28(8):848-855.
7. Kim K, Doi A, Wen B, et al. Epigenetic memory in induced pluripotent stem cells [in English]. *Nature*. 2010;467(7313):285-290.
8. Probst AV, Dunleavy E, Almouzni G. Epigenetic inheritance during the cell cycle. *Nat Rev Mol Cell Biol*. 2009;10(3):192-206.
9. Bestor TH. The DNA methyltransferases of mammals. *Hum Mol Genet*. 2000;9(16):2395-2402.
10. Li E, Bestor TH, Jaenisch R. Targeted mutation of the DNA methyltransferase gene results in embryonic lethality [in English]. *Cell*. 1992;69(6):915-926.
11. Okano M, Bell DW, Haber DA, Li E. DNA methyltransferases Dnmt3a and Dnmt3b are essential for de novo methylation and mammalian development [in English]. *Cell*. 1999;99(3):247-257.
12. Liao J, Karnik R, Gu HC, et al. Targeted disruption of DNMT1, DNMT3A and DNMT3B in human embryonic stem cells [in English]. *Nat Genet*. 2015;47(5):469-478.
13. Kaelin WG Jr, McKnight SL. Influence of metabolism on epigenetics and disease. *Cell*. 2013;153(1):56-69.
14. Carey BW, Finley LW, Cross JR, et al. Intracellular alpha-ketoglutarate maintains the pluripotency of embryonic stem cells. *Nature*. 2015;518(7539):413-416.
15. TeSlaa T, Chaikovsky AC, Lipchina I, et al. Alpha-Ketoglutarate accelerates the initial differentiation of primed human pluripotent stem cells. *Cell Metab*. 2016;24(3):485-493.
16. Wallace DC, Fan WW. Energetics, epigenetics, mitochondrial genetics [in English]. *Mitochondrion*. 2010;10(1):12-31.
17. Mahato B, Home P, Rajendran G, et al. Regulation of mitochondrial function and cellular energy metabolism by protein kinase C-lambda/tau: a novel mode of balancing pluripotency [in English]. *Stem Cells*. 2014;32(11):2880-2892.
18. Staerk J, Dawlaty MM, Gao Q, et al. Reprogramming of human peripheral blood cells to induced pluripotent stem cells. *Cell Stem Cell*. 2010;7(1):20-24.
19. Cong L, Ran FA, Cox D, et al. Multiplex genome engineering using CRISPR/Cas systems [in English]. *Science*. 2013;339(6121):819-823.
20. Chen ZX, Mann JR, Hsieh CL, Riggs AD, Chédin F. Physical and functional interactions between the human DNMT3L protein and members of the de novo methyltransferase family [in English]. *J Cell Biochem*. 2005;95(5):902-917.
21. Oceguera-Yanez F, Kim SI, Matsumoto T, et al. Engineering the AAVS1 locus for consistent and scalable transgene expression in human iPSCs and their differentiated derivatives. *Methods*. 2016;101:43-55.
22. Kotin RM, Linden RM, Berns KI. Characterization of a preferred site on human chromosome 19q for integration of adeno-associated virus DNA by non-homologous recombination. *EMBO J*. 1992;11(13):5071-5078.
23. Caglayan SHA, Cieslar-Pobuda A, Jensen V, et al. Optic atrophy 1 controls human neuronal development by preventing aberrant nuclear DNA methylation. *iScience*. 2020;23(6):101154.
24. Valente AJ, Maddalena LA, Robb EL, Moradi F, Stuart JA. A simple ImageJ macro tool for analyzing mitochondrial network morphology in mammalian cell culture. *Acta Histochem*. 2017;119(3):315-326.
25. Westermann B. Bioenergetic role of mitochondrial fusion and fission. *Biochim Biophys Acta*. 2012;1817(10):1833-1838.
26. Westermann B. Mitochondrial fusion and fission in cell life and death. *Nat Rev Mol Cell Biol*. 2010;11(12):872-884.
27. Smirnova E, Shurland DL, Ryazantsev SN, van der Bliek AM. A human dynamin-related protein controls the distribution of mitochondria. *J Cell Biol*. 1998;143(2):351-358.
28. Bleazard W, McCaffery JM, King EJ, et al. The dynamin-related GTPase Dnm1 regulates mitochondrial fission in yeast. *Nat Cell Biol*. 1999;1(5):298-304.
29. Zhu Z, Li C, Zeng Y, et al. PHB associates with the HIRA complex to control an epigenetic-metabolic circuit in human ESCs. *Cell Stem Cell*. 2017;20(2):274-289.
30. Zhang XD, Boyer L, Jin MJ, et al. Metabolic reprogramming during neuronal differentiation from aerobic glycolysis to neuronal oxidative phosphorylation [in English]. *Elife*. 2016;5:e13374
31. Funes JM, Quintero M, Henderson S, et al. Transformation of human mesenchymal stem cells increases their dependency on oxidative phosphorylation for energy production. *Proc Natl Acad Sci USA*. 2007;104(15):6223-6228.

SUPPORTING INFORMATION

Additional supporting information may be found online in the Supporting Information section at the end of this article.

How to cite this article: Cieslar-Pobuda A, Ahrens TD, Caglayan S, Behringer S, Hannibal L, Staerk J. DNMT3B deficiency alters mitochondrial biogenesis and α-ketoglutarate levels in human embryonic stem cells. *Stem Cells*. 2020;38:1409–1422. https://doi.org/10.1002/stem.3256